Please do not adjust margins

ARTICLE

Injection-seeded high-repetition-rate short-pulse micro-laser based on upconversion nanoparticles

Jiannan Jiao,[†,a] Donglei Zhou,[†,a] Shufan Li,[a] Mun Ji Low,[a] Yi Gao,[a] Jianing An,[a] Pei-Chen Su,[a] Seung-Woo Kim,[b] Seungchul Kim,[c,d] Kyujung Kim,[c,d] C. S. Suchand Sandeep,[*,a] and Young-Jin Kim [*,a,b]

We demonstrate a high repetition-rate upconversion green pulsed micro-laser, which is fabricated by fast thermal quenching of lanthanide-doped upconversion nanoparticles (UCNPs) via femtosecond-laser direct writing. The outer rim of the fabricated upconversion hemi-ellipsoidal microstructure works as a whispering-gallery-mode (WGM) optical resonator for coherent photon build-up of the third-harmonic ultra-short seed pulses. When near-infrared (NIR) femtosecond laser pulses of wavelength 1545 nm are focused onto the upconversion WGM resonator, the optical third-harmonic is generated at 515 nm together with upconversion luminescence. The weak third-harmonic (TH) seed pulses are coherently amplified in the hemi-ellipsoidal upconversion resonator as a result of the resonant interaction between the incident femtosecond laser field, the TH, the upconversion luminescence and the WGM. This upconversion lasing preserves the original repetition rate of the NIR pump laser and the output polarization state is also coherently aligned to the pump laser polarization. Because of the isotropic nature of the upconversion micro-ellipsoids, the upconversion lasing shows maximum intensity with linearly polarized pump beam and minimum intensity with circularly polarized pump beam. Our scheme devised for realizing high-repetition-rate lasing at higher photon energies in a compact micro platform will open up new ways for on-chip optical information processing, high-throughput microfluidic sensing, and localized micro light sources for optical memories.

1 Introduction

Upconversion (UC) luminescence in lanthanide-doped materials enables the emission of higher energy photons by optical excitation with lower energy photons via sequential absorption process. This UC emission process is attractive for various applications including data storage, multi-color displays, photovoltaic devices, and biological imaging [1-3]. Another promising way of generating higher energy photons from lower energy photons is by optical harmonic generation (HG). HG is a coherent nonlinear optical process that generates higher energy photons of integer multiples of the input photon energy. HG has been extensively researched because of its unique capability for generating ultrashort pulses, even down to attoseconds [4-6]. However, the power conversion efficiency of HG is generally very low. Recently, coherent amplification of HG from a UC nanoparticle (UCNP) thin-film was demonstrated by the authors, offering the potential to improve the power conversion efficiency [7]. As most materials exhibit a non-vanishing third-order susceptibility [4, 8, 9], lanthanide-doped systems could potentially work as promising gain media for visible output wavelengths when pumped by near-infrared (NIR) ultrashort pulses.

Manipulation of photons at micro-scale structures is the prerequisite for next-generation integrated photonics [10-12], micro-scale lasers [13-15], on-chip information processing [16, 17], and high-throughput biomedical sensing [15, 18-20]. The most commonly used micro-cavity structures in this regard are the Fabry-Perot cavity, photonic crystal cavity, and Whispering-gallery mode (WGM) cavity [18]. Out of these, WGM, formed by the light trapped at the boundary of a symmetrical dielectric structure via total internal reflection, provides a high quality factor (Q-factor) over 10^9 for both solid and liquid resonators [21-23]. Different geometries including spheres, hemispheres, rings, and disks have been used for forming WGM cavities [24] using various materials such as proteins [25], fluorescent dyes [12, 26, 27], perovskites [28, 29], UCNPs [3], and organic-inorganic hybrid materials [30]. Diverse manufacturing techniques have been employed for the fabrication of WGM cavities [31]. Out of them, femtosecond-laser direct writing (FsLDW) based on the additive manufacturing concept (also known as 3D printing), is highly promising for the fabrication of precise micro-cavities and micro-lasers owing to its unique sub-micron printing resolution (even beyond the optical diffraction limit) enabled by two-photon polymerization process [32-35]. FsLDW also helps in reducing the manufacturing time compared to other traditional 3D printing methods [36, 37].

In this paper, we report high-repetition-rate short-pulse lasing from an upconversion micro-sized, hemi-ellipsoidal optical cavity fabricated by the fast thermal quenching of UCNPs. The ultrafast quenching enabled by femtosecond laser pulses results in a micro-

[a] Singapore Centre for 3D Printing, School of Mechanical and Aerospace Engineering, Nanyang Technological University (NTU), 50 Nanyang Avenue, 639798, Singapore. E-mail: ssuchand@ntu.edu.sg, yj.kim@kaist.ac.kr
[b] Department of Mechanical Engineering, Korea Advanced Institute of Science and Technology (KAIST), Science Town, Daejeon, 34141 South Korea
[c] Department of Cogno-mechatronics Engineering, Pusan National University, Busan, 46241, South Korea
[d] Department of Optics and Mechatronics Engineering, Pusan National University, Busan, 46241, South of Korea
†These authors contributed equally to this work

ellipsoidal cavity with a highly smooth surface. Upconversion-luminescence-assisted WGM lasing at green wavelength is achieved when the hemi-ellipsoidal cavity is pumped by NIR femtosecond laser pulses. The narrowest spectral bandwidth of our micro-laser reaches down to a full width at half maximum (FWHM) of 3.0 nm at a high repetition of 83.3 MHz. The measurements on the lasing intensity dependence to input polarization states show that harmonic generation contributes to the lasing, and the input pump beam should be linearly polarized to get the most efficient lasing. This high repetition-rate short-pulse laser will open up a broad range of engineering and industrial applications, such as automated inspection, biological imaging, high-speed circuit testing, and healthcare applications [38, 39].

2 Experiments: sample patterning and test setup

2.1 Fabrication of hemi-ellipsoidal UC microstructure patterned by FsLDW

The $NaYF_4$:Yb^{3+},Er^{3+} UCNPs are synthesized using a typical solvothermal method [40] as follows. 0.2 mmol YbCl3•6H2O, 0.78 mmol YCl_3•$6H_2O$ and 0.02 mmol $ErCl_3$•$6H_2O$ are added to a solution containing 15 mL 1-octadecene and 6 mL oleic acid. The mixture is heated to 160 °C to remove residual water and oxygen, and the resultant pellucid solution is cooled down to room temperature. To this pellucid solution, 10 mL of 2.5 mmol NaOH and 4 mmol NH_4F solution in methanol is slowly added and stirred for 30 minutes. The resultant solution is then heated to 80 °C for 30 minutes to evaporate methanol from the reaction mixture. Subsequently, the temperature is raised to 320 °C and maintained for 1 hour under argon atmosphere. The solution is then cooled down to the room temperature and an excess of ethanol is added. The resultant mixture is centrifugally separated, the precipitate collected is washed three times with ethanol, and finally oven-dried at 60 °C. To fabricate the UC micro-ellipsoids using FsLDW, a thin film of the $NaYF_4$:Yb^{3+},Er^{3+} UCNP is prepared using the interfacial assembly method. A glass substrate is immersed vertically into a solution of 1 mmol colloidal $NaYF_4$:Yb^{3+},Er^{3+} UCNP in cyclohexane. With the slow volatilization of cyclohexane, the $NaYF_4$:Yb^{3+},Er^{3+} UCNPs are self-organized onto the surface of the glass substrate. High energy UV femtosecond laser pulses are used to fast quench the UCNP film to form the UC micro-ellipsoids as shown in Fig. 1a. The insets of Fig. 1a show the transmission electron microscope (TEM) image and scanning electron microscope (SEM) image of the synthesized UCNPs which are later fast quenched to form the micro-ellipsoids. It can be seen that the $NaYF_4$:Yb^{3+},Er^{3+} UCNPs are well-crystallized and display uniform hexagonal shape with an average particle size of 25 nm.

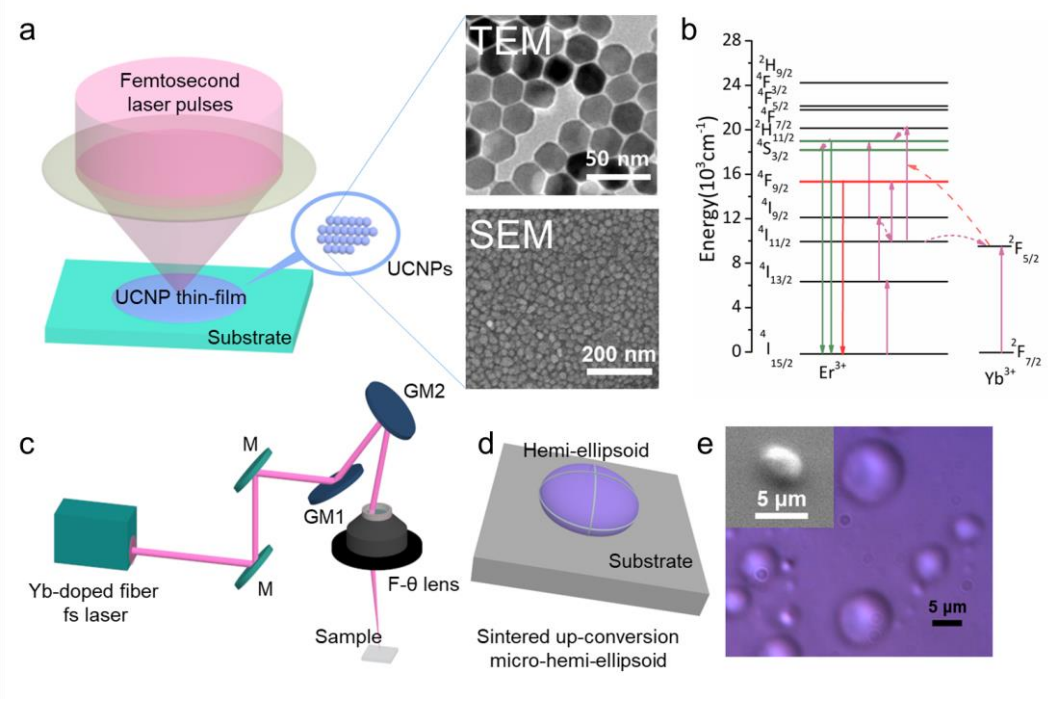

Fig. 1 Fabrication of upconversion micro-lasing structure using high-speed femtosecond laser direct writing. (a) Schematic for sintering of UC micro-ellipsoids. The inset shows TEM and SEM images of the synthesized UCNPs. (b) Energy level diagram of $NaYF_4$:Yb^{3+},Er^{3+} UCNPs. (c) Schematic of the femtosecond laser direct writing system. (d) Schematic of the micro-ellipsoid structure. (e) Optical microscope and SEM (inset) images of the fabricated UC micro hemi-ellipsoids. Abbreviations: M: mirror, and GM: Galvano mirror.

Fig. 1b shows the energy diagram for the UC luminescence of $NaYF_4$:Yb^{3+},Er^{3+}. Upon excitation of the UCNPs, the electrons in the ground state, $^4I_{15/2}$ are first excited to $^4I_{13/2}$ state through ground state absorption, and are then further pumped to $^4I_{9/2}$ via the excited state absorption. The electrons in the $^4I_{9/2}$ state can either relax to $^4I_{11/2}$ non-radiatively or get pumped to $^2H_{11/2}$/$^4S_{3/2}$ state, generating green $^2H_{11/2}$/$^4S_{3/2}$–$^4I_{15/2}$ transitions. The electrons on $^4I_{11/2}$ gets pumped to $^4F_{9/2}$, generating the red emission of $^4F_{9/2}$–$^4I_{15/2}$ [41, 42], or are excited to $^2H_{11/2}$/$^4S_{3/2}$, generating green emissions of $^2H_{11/2}$/$^4S_{3/2}$–$^4I_{15/2}$. Additionally, through the non-radiative process, $^2F_{7/2}$+$^4I_{11/2}$ →$^2F_{5/2}$+$^4I_{15/2}$, the excited state energy of $^4I_{11/2}$ can be transferred to Yb^{3+}. The Yb^{3+} ions on $^2F_{5/2}$ can help to pump Er^{3+} ions on $^4I_{11/2}$ to the higher excited state $^4F_{7/2}$ through back energy transfer from Yb^{3+} to Er^{3+} [43, 44]. The electrons on $^4F_{7/2}$ level can relax to the $^2H_{11/2}$/$^4S_{3/2}$ level, which further contributes to the green emissions of $^2H_{11/2}$/$^4S_{3/2}$–$^4I_{15/2}$. The energy gap between $^4F_{9/2}$ and $^4F_{5/2}$ is 0.85 eV, which is higher than the energy (0.80 eV) of the 1545 nm pump light. Therefore, the possibility of excited-state absorption (ESA) from $^4F_{9/2}$ to $^4F_{5/2}$ is quite low. However, the ESA from $^4I_{9/2}$ to $^2H_{11/2}$ is quite possible, which further contributes to the green emission. Therefore, the green emission constitutes the main part of the upconversion spectrum. It should be noted that the third harmonic of the pump laser also falls in this green emission region. This leads to the resonance of the incident NIR femtosecond laser, its third harmonic, the UC luminescence, and the WGM cavity mode to facilitate the UC lasing process.

Fig. 1c shows the layout of the FsLDW system used for the fabrication of the UC micro-ellipsoids. Third harmonic from a Yb-doped fiber femtosecond laser (Amplitude Systems, Satsuma HP) at 343 nm with 220 fs pulse duration at a repetition rate of 500 kHz is used for the FsLDW. The laser beam is tightly focused and scanned along the UCNP film to fabricate the micro-ellipsoids. The average size of the micro hemi-ellipsoids can be controlled by tailoring the laser power and the scanning speed. Fig. 1d shows the schematic of the micro-ellipsoidal structure and Fig. 1e shows the actual micro-ellipsoids fabricated using different scan speeds at the laser power of 11 mW using the FsLDW system.

2.2 Optical configuration for upconversion lasing

The experimental setup used for UC lasing from the UC hemi-ellipsoids is presented in Fig. 2a. Femtosecond laser pulses from an Er-doped femtosecond fiber laser (Toptica FemtoFiber pro SCIR, 100 fs, 83.3 MHz) with an average power of 170 mW at 1545 nm center wavelength are focused to the edge of the sintered UC hemi-ellipsoid. To remove any residual short-wavelength light present in the excitation beam, an 800 nm long-pass filter (Thorlabs FELH0800) is positioned in front of the focusing objective lens. A 40× objective lens (Newport LI-40X) with a numerical aperture (NA) of 0.65 is used to focus the input beam to a small spot of 7.6 µm diameter (FWHM) onto the sample. A 20× objective lens (Olympus LUCPLFLN 20X, 0.45 NA) is used to collect the emission from the UC micro-ellipsoids. The excitation wavelength is filtered from the emission spectrum using a 750 nm short-pass filter (Thorlabs FES0750). The emission collected is directed to a broadband spectrometer (Andor Shamrock 193i) coupled to a highly-sensitive electron-multiplying charge coupled device (EMCCD, Andor IXon Ultra) for spectral analysis. A compact CMOS color camera (Thorlabs, DCC1645C) is used for capturing images of the sample and the WGM patterns. The radio-frequency (RF) domain analysis of the UC lasing is realized by a photomultiplier tube (PMT: Thorlabs PMT1001M) connected to an RF spectrum analyzer (RIGOL DSA875).

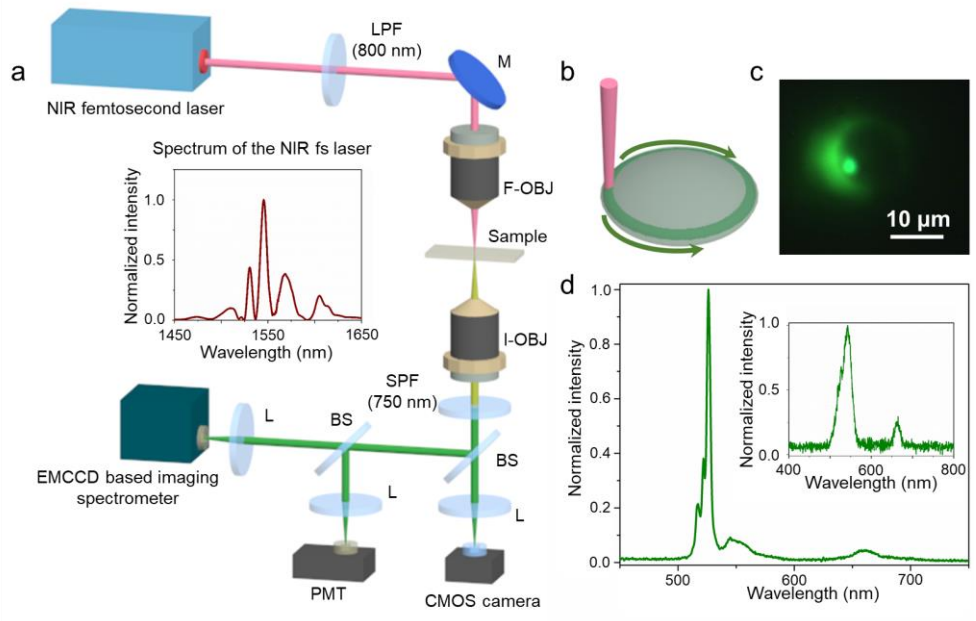

Fig. 2 Optical configuration for the observation of UC lasing. (a) Optical layout of characterization system using a femtosecond pump laser of 1545 nm center wavelength. (b) Schematic for femtosecond laser induced WGM process. (c) WGM pattern observed from a micro-ellipsoid of 10 µm. (d) Lasing spectrum of the WGM resonance. The inset shows the spectrum of UC luminescence of the UCNP film. Abbreviations: LPF: long-pass filter, M: mirror, F-OBJ: focusing objective, I-OBJ: imaging objective, SPF: short-pass filter, BS: beam splitter, L: lens, CMOS camera: compact complementary metal oxide semiconductor camera, PMT: photomultiplier tube, EMCCD: electron multiplying charge-coupled device.

By focusing the pump light on to the edge of the smooth UC micro-ellipsoids, the WGM resonance can be achieved. Fig. 2b shows the schematic of the WGM resonance and Fig. 2c shows the microscope color image of WGM from the sample. The WGM in a given resonator depends only on the geometry of the resonator, and is independent of the gain medium [24]. A bright ring-shaped pattern is observed at the outer boundary, indicating the distribution of the electric field and the formation of WGM resonances. The UC lasing spectrum with the lasing peak at 526 nm is shown in Fig. 2d; the inset shows the UC luminescence of the UCNP film with emission peaks at 543 nm and 665 nm.

3 Results and discussion

3.1 Upconversion lasing spectra from a UC hemi-ellipsoidal resonator

To characterize the UC lasing from the hemi-ellipsoidal structure, an EMCCD with controllable input slit width is used to capture the emission spectra from different observation areas of the sample. As shown in Fig. 3a, the narrow-width slit is aligned to look at the edge of the hemi-ellipsoid (of 10 μm diameter) to capture the lasing from the WGM ring pattern when the input beam pumped at the edge of the ellipsoid. Fig. 3b shows the normalized lasing spectrum at 534 nm with a narrow bandwidth of 3.0 nm from the hemi-ellipsoid, when pumped with a pulse energy of 2.5 nJ. The slit width is 100 μm, so the actual imaging area is 5.0 μm considering the magnification of the 20× imaging objective. The lasing spectrum has a Gaussian distribution with an R^2 value of 0.9996. Fig. 3c shows the RF spectrum of the UC laser pulse train signal obtained by an RF spectrum analyzer connected to the high-speed PMT. The UC lasing has a pulse repetition rate of 83.3 MHz, which is the same as the input femtosecond pulses, corresponding to the pulse-to-pulse time spacing of 12 ns.

The dependence of the UC lasing intensity on the pump energy is shown in Fig. 3d. The slope change in the emission intensity occurs when the pump energy reaches 1.86 nJ, which corresponds to the lasing threshold. Fig. 3e shows the bandwidth change of the lasing spectrum with different pump energies. The FWHM of the lasing bandwidth decreases as the pump energy increases, and reaches a minimum of 3.0 nm. The typical "S" shaped log-log plot of the emission intensity *vs* excitation energy (see Fig. 3d), and the flattening of the emission bandwidth (see Fig. 3e) confirms the lasing emission. When the slit width before the EMCCD increases, the wider part of the hemi-ellipsoid can be captured and UC luminescence peaks start to be observed. As shown in Fig. 3f, when the slit width increases from 100 μm to 300 μm, the UC luminescence emission peaks at 548 nm and 661 nm become visible.

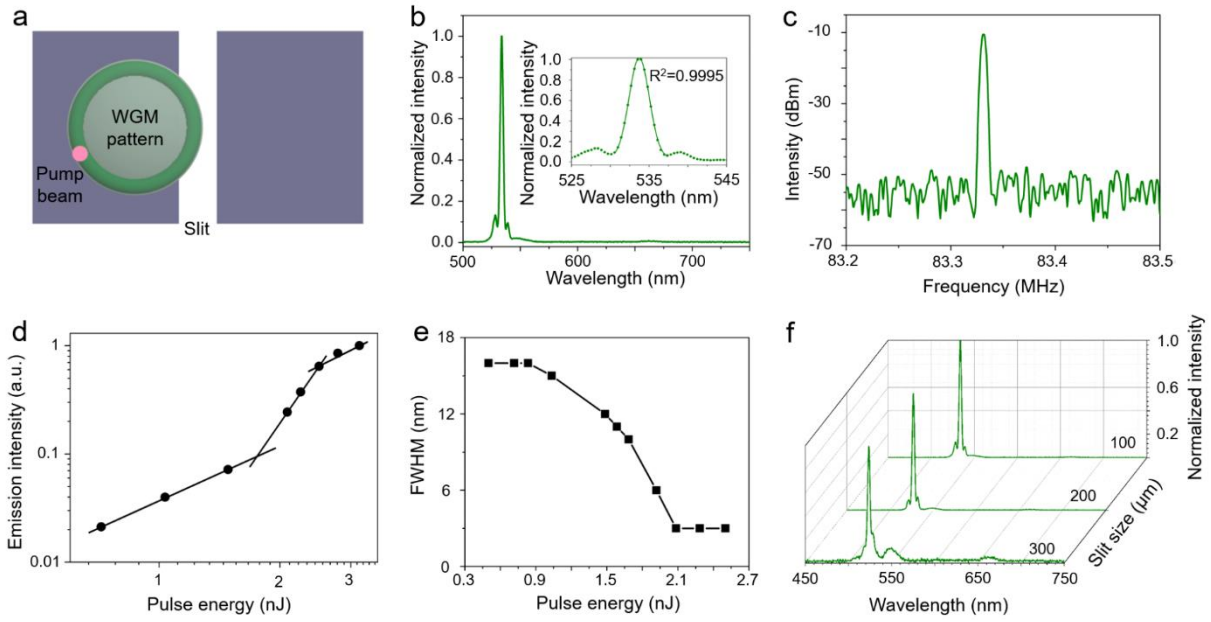

Fig. 3 Characterization of the UC lasing spectrum with different EMCCD slit widths. (a) Schematic for the observation of UC lasing through an adjustable slit. (b) UC lasing spectrum using a narrow slit aligned to the edge of the WGM pattern. Inset shows the Gaussian fitting of the lasing spectrum. (c) RF domain characteristics of the lasing spectrum. (d) Dependence of the UC emission intensity on the input pump energy. (e) Dependence of the UC emission bandwidth on the input pump energy. (f) Spectral distributions captured with different EMCCD slit widths. With larger slit widths, emission from the entire structure can be collected, which also shows the UC luminescence emission peaks.

3.2 Comparison of upconversion lasing and upconversion luminescence spectrum

Fig. 4 shows the pump position and input pulse energy dependence of UC lasing and UC luminescence spectrum from a larger hemi-ellipsoid of 15.6-μm diameter. A larger slit width of 1,000 μm is used in this case to capture both UC lasing and UC luminescence from the hemi-ellipsoid. For investigating the pump position dependence, the input pump beam position is translated from the center to the edge of the hemi-ellipsoid, while corresponding emission spectra are recorded. The emission from the un-sintered UCNP film is used as the reference. As shown in Fig. 4a and Fig. 4b, when pumped at the center or outside of the hemi-ellipsoid structure, only UC luminescence and THG emission (515 nm) can be observed. In contrast, when the pump laser is focused at the edge of the hemi-ellipsoid, lasing peaks at 521 nm and 514 nm can be observed, owing to WGM resonance. The emission wavelength of this WGM resonance based UC lasing is dependent on the cavity geometry. This causes the shift in the emission wavelength in the cases where the UCNP hemi-ellipsoid is pumped close to the edge. However, UC luminescence peaks remain unchanged at 535 nm and 651 nm regardless of the pump position. The peak power of lasing (521 nm) is 5.73×10^{-6} mW when the pumping energy is 136 mW, corresponding to a laser conversion efficiency of 4.2×10^{-8}. When the hemi-ellipsoid is small enough to be covered completely by the pump beam, a stable lasing spectrum, independent of slit width can be obtained. Fig. 4b inset shows the stable lasing spectra from a small hemi-ellipsoid of 5 μm diameter with the lasing emission peak at 535 nm recorded with different slit widths. The EMCCD slit width is varied between 80 μm to 1000 μm and the emission spectra remains stable throughout. Fig. 4c shows the emission spectra from the UC hemi-ellipsoid when different pump energies are focused to the edge of the hemi-ellipsoid. Fig. 4d shows the intensity dependence of different emission peaks on the pump energy. For the lasing emission peaks at 521 nm and 514 nm, the slope sharply changes at the threshold of 0.8 nJ/pulse due to the stimulated emission, whereas the intensity of UC luminescence (at 535 nm and 651 nm) shows a linear dependence on the pump energy without lasing.

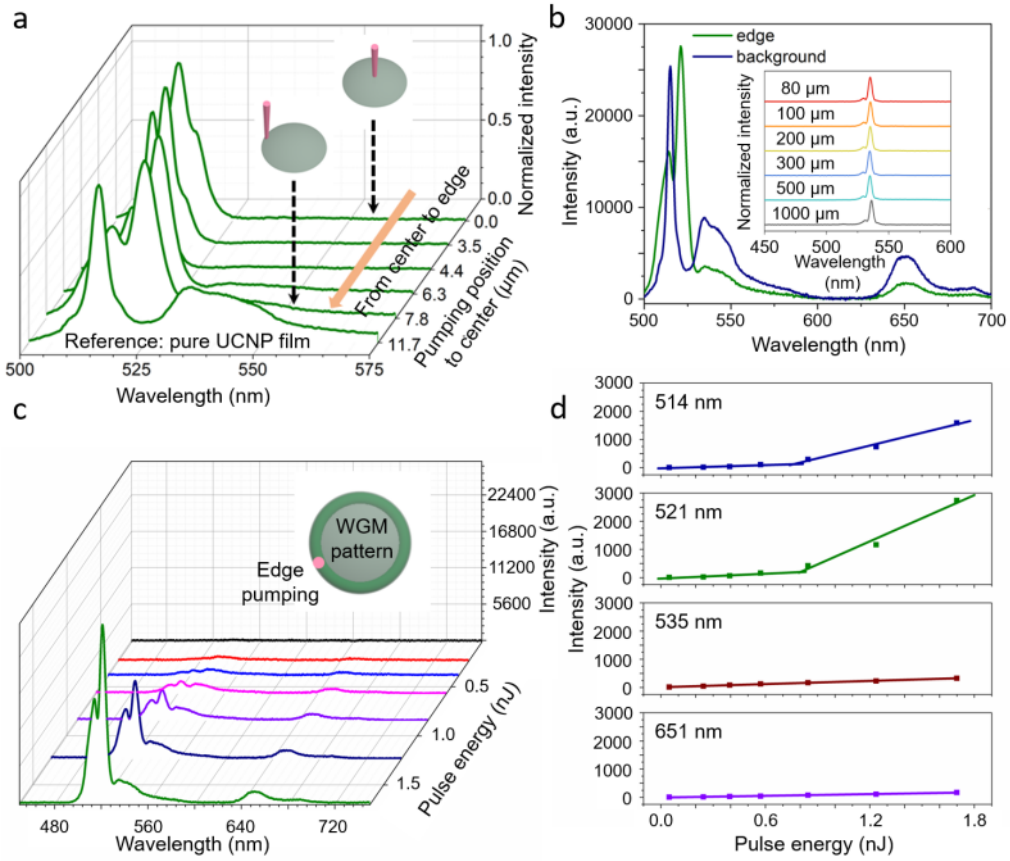

Fig. 4 UC lasing and UC luminescence spectra for different pumping positions and pump energies. (a) Normalized emission spectra when the hemi-ellipsoid was pumped at different positions. (b) Comparison of the lasing spectrum obtained by pumping at the edge of the hemi-ellipsoid with the emission spectrum obtained from the unsintered UCNP film. Inset shows the slit width independent UC lasing spectrum for a uniformly pumped hemi-ellipsoid of 5 μm diameter. (c) Evolution of the lasing emission with different pump energies. (d) Pump energy dependence of the UC lasing and UC luminescence spectra.

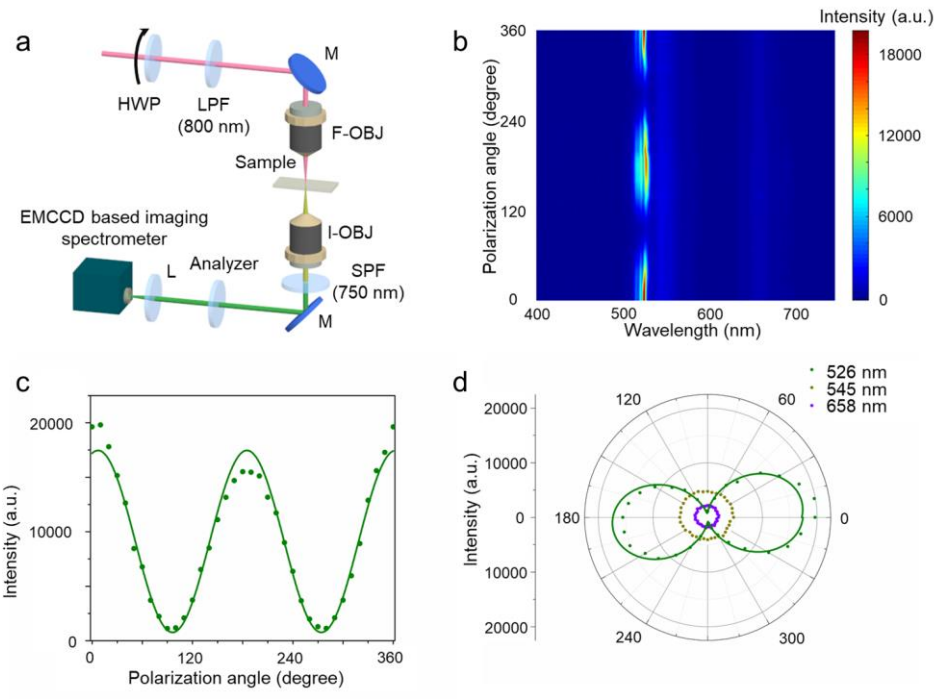

Fig. 5 Measurement of polarization direction of UC lasing. (a) Schematic of the measurement system used for characterizing the polarization direction of UC lasing. (b) Intensity distribution of the emission spectrum from the hemi-ellipsoid recorded through an analyser for different linear polarization directions of the pump laser. (c) Linear pump polarization dependent intensity of the UC lasing wavelength recorded through the analyser. (d) Polar plot of UC lasing and UC luminescence for different input linear polarization directions. The intensity of UC luminescence is magnified by a factor of 3 in this plot. Abbreviations: HWP: half-wave plate, LPF: long-pass filter, M: mirror, F-OBJ: focusing objective, I-OBJ: imaging objective, L: lens SPF: short-pass filter, and EMCCD: electron multiplying charge-coupled device.

3.3 Polarization of UC lasing when pumped with a linearly polarized beam

A half-wave plate is inserted in the pump beam as shown in Fig. 5a, and the linear polarization direction of the incident pump is changed by rotating the half-wave plate. The polarization direction of the lasing emission is evaluated using a polarizer. The half-wave plate is rotated with a 5° step while the analyzer is kept fixed, so that different polarization directions result in different intensities after passing through the analyzer. From Fig. 5b, one can confirm that the polarization direction at lasing wavelength (526 nm) from the hemi-ellipsoid is directly dependent on the input polarization; the polarization parallel to the transmission direction of the analyzer shows the maximum intensity. Because the seed light is made by THG, the lasing emission will have the same polarization with the THG, which in turn has the same polarization of the input laser. Fig. 5c shows the UC lasing emission intensity depending on the input linear polarization state. In contrast, the UC luminescence polarization (545 nm and 658 nm) has no dependency on the pump laser's polarization direction, as shown in Fig. 5d.

3.4 Measurement of UC lasing intensity with different elliptical pump polarizations

To investigate the lasing emission intensity dependence on input polarization states, a quarter-wave plate is inserted to the input beam path; the ellipticity of the input pump polarization is varied by rotating the quarter-wave plate while keeping the half-wave plate as is (see Fig. 6a). The analyzer is removed from the detection path herein. The quarter-wave plate is rotated in 5° steps from the initial position, 0° (the position at which the fast axis of the quarter-wave plate is parallel to the fast axis of the half-wave plate). Fig. 6b shows the intensity distribution of the emission spectrum from the hemi-ellipsoid with different pump polarization ellipticities. Fig. 6c shows the UC lasing peak's (520 nm) intensity dependence on the pump polarization ellipticity. The lasing intensity reaches the minimum when the rotation angle of the quarter-wave plate is either 45° or 135°, where the pump beam is circularly polarized. The lasing intensity reaches the maximum when the pump laser is linearly polarized corresponding to the rotation angles of the quarter-wave plate; 0°, 90° or 180°. On the contrary, there is no pump ellipticity dependence in UCL emissions, as shown in Fig. 6d. Due to the isotropic nature of the UC hemi-ellipsoid structure, the nonlinear polarization components for THG disappear for the circularly polarized beam in the hemi-ellipsoid [8]. This implies that the seed THG will not be present in circular polarization pumping, and hence no UC lasing occurs for circularly polarized pump beam. Therefore, for obtaining the best efficiency in UC lasing, a linearly polarized pump beam should be used and be pumped onto the edge of the UC hemi-ellipsoids.

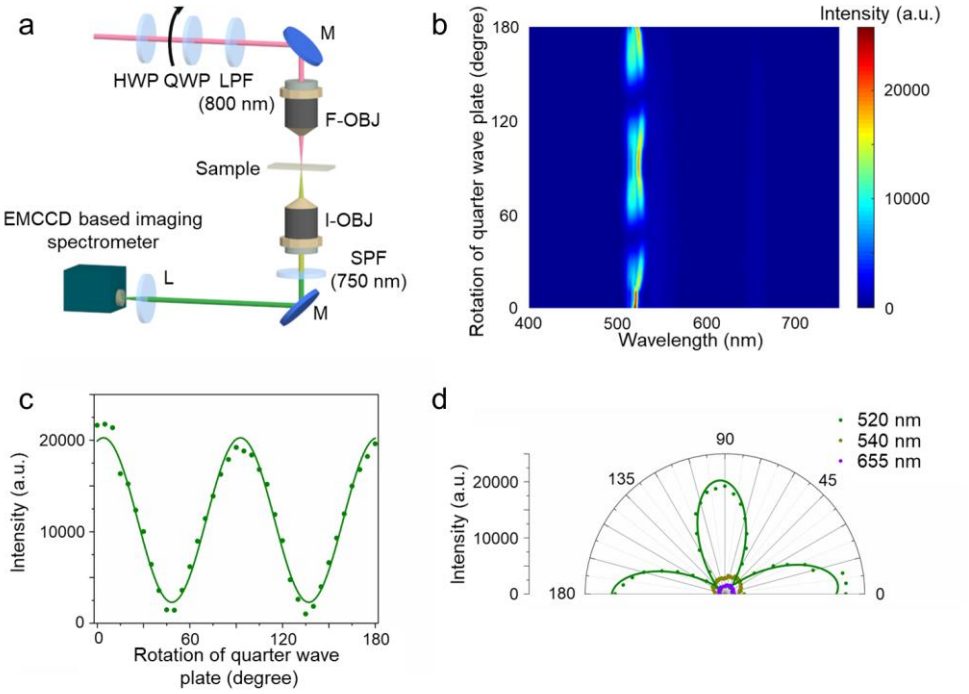

Fig. 6 Dependence of UC lasing intensity on different pump polarization ellipticities. (a) System schematic for measuring UC lasing intensity with different pump ellipticities. (b) Intensity distribution of the emission spectrum with different polarization ellipticities of the pump beam. (c) Dependence of the UC lasing intensity on input pump ellipticities (d) Polar plot of the UC lasing peak and UC luminescence peaks for different input polarization ellipticities. The UC luminescence intensity is magnified by a factor of 3. Abbreviations: HWP: half-wave plate, QWP: quarter-wave plate, LPF: long-pass filter, M: mirror, F-OBJ: focusing objective, I-OBJ: imaging objective, SPF: short-pass filter, L: lens and EMCCD: electron multiplying charge-coupled device.

4 Conclusions

In conclusion, UC lasing at high repetition rates from micro-sized UC hemi-ellipsoids was achieved. UC hemi-ellipsoids of different diameters were fabricated using a programmable FsLDW system. The resulting smooth convex hemi-ellipsoids work as WGM resonators. When intense NIR femtosecond laser pulses are focused onto this WGM resonator, they generate optical third-harmonic of the pump laser beam. At the same time, the NIR pulses also work as the pump light for the upconversion processes to generate UC luminescence. The weak third-harmonic act as the seed beam and are coherently amplified in the hemi-ellipsoidal UC WGM resonator. The lasing wavelength is found to be strongly dependent on the size of the hemi-ellipsoidal cavity due to the WGM resonance. The output wavelength is determined, therefore, by the overlap between the THG of the NIR femtosecond laser, the UC luminescence, and the WGM resonance, which makes the output wavelength to be slightly shifted from the central wavelength of the third harmonic. UC lasing emission from the hemi-ellipsoid of 10 μm diameter occurs at a pump threshold of 1.86 nJ and can reach down to a narrow bandwidth of 3.0 nm. The upconversion lasing has a pulse-to-pulse spacing of 12 ns (corresponding to a repetition rate of 83.3 MHz) that follows the pump laser's repetition rate. It is well known that THG, being a pure electronic nonlinear process, is instantaneous and follows the exact repetition rate and pulse width of the pump laser. As the observed UC lasing is generated from the coherent interaction of the UC luminescence with the THG, it also follows the same repetition rate as the THG, namely 83.3 MHz. Due to the isotropic nature of the UC microstructures, the highest lasing intensity occurs with linearly polarized pumping, and the lowest with circularly polarized pumping. This high repetition rate UC lasing at higher photon energies in a compact micro-sized platform will open up new perspectives for on-chip information processing, high-throughput microfluidic sensing, and localized micro sources for optical memories.

Conflicts of interest

There are no conflicts to declare.

Acknowledgements

The authors acknowledge funding support received from Panasonic Factory Solutions Asia Pacific (PFSAP) and Singapore Centre for 3D Printing (RCA-15/027), National Research Foundation of the Republic of Korea (NRF-2012R1A3A1050386, NRF-2018R1A4A1025623), Korea Forest Service (Korea Forestry Promotion Institute) through the R&D Program for Forest Science Technology (2020229C10-2022-AC01), and Basic Research Program (NK224C) funded by the Korea Institute of Machinery and Materials.

References

1. C. Altavilla, *Upconverting nanomaterials: perspectives, synthesis, and applications*, CRC Press, Boca Raton, FL, 2016.
2. H. Zhu, X. Chen, L. M. Jin, Q. J. Wang, F. Wang and S. F. Yu, *ACS*

nano, 2013, **7**, 11420-11426.
3. A. Fernandez-Bravo, K. Yao, E. S. Barnard, N. J. Borys, E. S. Levy, B. Tian, C. A. Tajon, L. Moretti, M. V. Altoe and S. Aloni, *Nat. Nanotechnol.*, 2018, **13**, 572.
4. R. W. Boyd, *Nonlinear Optics*, Academic Press, London, 2003.
5. M. Kauranen and A. V. Zayats, *Nat. Photonics*, 2012, **6**, 737.
6. B. E. Saleh and M. C. Teich, *Fundamentals of photonics*, John Wiley & Sons, Hoboken, NJ, 2019.
7. Y. Gao, H. Lee, W. Xu, J. Jiao, P. Chen, D.-H. Kim and Y.-J. Kim, *Sci. Rep.*, 2019, **9**, 5094.
8. J. Jiao, Y. Gao, S. Li, N. D. Anh, P.-C. Su, S.-W. Kim, C. S. Sandeep and Y.-J. Kim, *Opt. Express*, 2019, **27**, 29196-29206.
9. T. Y. Tsang, *Phys. Rev. A*, 1995, **52**, 4116.
10. J. L. O'brien, A. Furusawa and J. Vučković, *Nat. Photonics*, 2009, **3**, 687.
11. M. Law, D. J. Sirbuly, J. C. Johnson, J. Goldberger, R. J. Saykally and P. Yang, *Science*, 2004, **305**, 1269-1273.
12. C. Zhang, C.-L. Zou, Y. Zhao, C.-H. Dong, C. Wei, H. Wang, Y. Liu, G.-C. Guo, J. Yao and Y. S. Zhao, *Sci. Adv.*, 2015, **1**, e1500257.
13. Q. Zhang, R. Su, W. Du, X. Liu, L. Zhao, S. T. Ha and Q. Xiong, *Small Methods*, 2017, **1**, 1700163.
14. K. An, J. J. Childs, R. R. Dasari and M. S. Feld, *Phys. Rev. Lett.*, 1994, **73**, 3375.
15. M. T. Hill and M. C. Gather, *Nat. Photonics*, 2014, **8**, 908.
16. M. Ferrera, Y. Park, L. Razzari, B. E. Little, S. T. Chu, R. Morandotti, D. J. Moss and J. Azaña, *Nat. Commun.*, 2010, **1**, 29.
17. F. Flamini, N. Spagnolo and F. Sciarrino, *Rep. Prog. Phys.*, 2018, **82**, 016001.
18. W. Zhang, J. Yao and Y. S. Zhao, *Acc. Chem. Res.*, 2016, **49**, 1691-1700.
19. J. T. Robinson, L. Chen and M. Lipson, *Opt. Express*, 2008, **16**, 4296-4301.
20. S. Soria, S. Berneschi, M. Brenci, F. Cosi, G. Nunzi Conti, S. Pelli and G. C. Righini, *Sensors*, 2011, **11**, 785-805.
21. L. He, Ş. K. Özdemir and L. Yang, *Laser Photonics Rev.*, 2013, **7**, 60-82.
22. A. A. Savchenkov, A. B. Matsko, V. S. Ilchenko, I. Solomatine, D. Seidel and L. Maleki, *Phys. Rev. Lett.*, 2008, **101**, 093902.
23. S. Uetake, R. Sihombing and K. Hakuta, *Opt. Lett.*, 2002, **27**, 421-423.
24. T. Reynolds, N. Riesen, A. Meldrum, X. Fan, J. M. Hall, T. M. Monro and A. François, *Laser Photonics Rev.*, 2017, **11**, 1600265.
25. Y.-L. Sun, Z.-S. Hou, S.-M. Sun, B.-Y. Zheng, J.-F. Ku, W.-F. Dong, Q.-D. Chen and H.-B. Sun, *Sci. Rep.*, 2015, **5**, 12852.
26. J. Zhao, Y. Yan, Z. Gao, Y. Du, H. Dong, J. Yao and Y. S. Zhao, *Nat. Commun.*, 2019, **10**, 870.
27. J.-F. Ku, Q.-D. Chen, R. Zhang and H.-B. Sun, *Opt. Lett.*, 2011, **36**, 2871-2873.
28. W. Zhang, L. Peng, J. Liu, A. Tang, J. S. Hu, J. Yao and Y. S. Zhao, *Adv. Mater.*, 2016, **28**, 4040-4046.
29. J. Zhao, Y. Yan, C. Wei, W. Zhang, Z. Gao and Y. S. Zhao, *Nano Lett.*, 2018, **18**, 1241-1245.
30. P. Liu, X. He, J. Ren, Q. Liao, J. Yao and H. Fu, *ACS nano*, 2017, **11**, 5766-5773.
31. H. Chandrahalim, S. C. Rand and X. Fan, *Sci. Rep.*, 2016, **6**, 32668.
32. P.-I. Dietrich, M. Blaicher, I. Reuter, M. Billah, T. Hoose, A. Hofmann, C. Caer, R. Dangel, B. Offrein and U. Troppenz, *Nat. Photonics*, 2018, **12**, 241.
33. T. Gissibl, S. Thiele, A. Herkommer and H. Giessen, *Nat. Photonics*, 2016, **10**, 554.
34. S. Maruo and J. T. Fourkas, *Laser Photonics Rev.*, 2008, **2**, 100-111.
35. Y.-L. Zhang, Q.-D. Chen, H. Xia and H.-B. Sun, *Nano Today*, 2010, **5**, 435-448.
36. S. Magdassi and A. Kamyshny, *Nanomaterials for 2D and 3D Printing*, John Wiley & Sons, Weinheim, Germany, 2017.
37. K. Sugioka and Y. Cheng, *Lab Chip*, 2012, **12**, 3576-3589.
38. M. E. Fermann, A. Galvanauskas and G. Sucha, *Ultrafast lasers: technology and applications*, CRC Press, New York, USA, 2002.
39. C. Rulliere, *Femtosecond laser pulses*, Springer, New York, USA, 2005.
40. H.-X. Mai, Y.-W. Zhang, R. Si, Z.-G. Yan, L.-d. Sun, L.-P. You and C.-H. Yan, *J. Am. Chem. Soc.*, 2006, **128**, 6426-6436.
41. J. Zheng, X. F. Wang, W. Y. He, Y. Y. Bu and X. H. Yan, *Appl. Phys. B*, 2013, **115**, 443-449.
42. A. S. Gouveia-Neto, L. A. Bueno, R. F. do Nascimento, E. A. da Silva and E. B. da Costa, *J. Non. Cryst. Solids*, 2009, **355**, 488-491.
43. S. He, H. Xia, J. Zhang, Y. Zhu and B. Chen, *Sci. Rep.*, 2017, **7**, 8751.
44. W. Ahn and Y. J. Kim, *Opt. Mater. Express*, 2016, **6,** 257067 .